Characterizing OCO-2 XCO_2 Variability for the Conterminous United States and Adjacent Ocean

Kayla Alexis Mitchell
Durham, North Carolina

B.S., Appalachian State University, 2018

A Thesis presented to the Graduate Faculty
of the University of Virginia in Candidacy for the Degree of
Master of Science

Department of Environmental Sciences

University of Virginia
December, 2020

Abstract

We use a geostatistical framework to analyze new, high resolution, column-averaged CO_2 (XCO_2) measurements from NASA's Orbiting Carbon Observatory 2 (OCO-2) and provide a characterization of seasonal and sub-seasonal variability within XCO_2 over the conterminous United States and adjacent ocean basins. Of particular interest are the differences between land and ocean XCO_2 distributions, which are significant in CO_2 at the surface. Surface measurement networks have shown that surface CO_2 fluxes are greater and more variable over land. We investigate whether this contrast is reflected in XCO_2, for which large-scale transport generally obscures local fluxes. We show land and ocean seasonal XCO_2 variability is most divergent for the west coast and fairly smoothed across the east coast. Our results are mostly consistent with modeled XCO_2, showing a mean increasing north-south meridional pattern and high seasonal variability over areas affected by boreal carbon fluxes. The western United States has strikingly lower seasonal amplitudes than the adjacent Pacific Ocean and eastern United States. Higher latitudes in the domain tend to have greater seasonal amplitudes, and the highest seasonal amplitudes are over the Canadian Shield. Our results suggest synoptic-scale XCO_2 variance is driven primarily by advection across the mean meridional gradient, consistent with findings from the ground-based Total Carbon Column Observing Network (Keppel-Aleks et al., 2011). Synoptic-scale XCO_2 variance is greater (almost doubled for the west coast) over land than ocean, and greatest over the northwest and northeast. The impact of instrument and algorithm noise as well as small spatial-scale geophysical signals are evaluated by averaging adjacent retrievals

along-orbit and found to impart ~25% of the variability in XCO_2 data analyzed. There are certain incongruencies between our results and modeled or observed XCO_2 that prompt further investigation into the OCO-2 data as well as model representations of atmospheric transport and surface fluxes. Future work will focus on attributing the observed variability to real geophysical signals or residual bias in OCO-2 soundings. This analysis provides insight on real carbon cycle and atmosphere-driven XCO_2 variations and may be used to improve modeling and satellite retrieval techniques.

I would like to thank Scott Doney and Gretchen Keppel-Aleks for their expert guidance and warm encouragement, which was unwavering throughout a highly unusual and challenging year.

Thanks also to Yifan Guan and Anthony Torres of my research group for their help along the way.

I would not have reached this point without the support of my family. Thanks to Teresa, Robert, Ninna, Van, and Hayden.

I would also like to thank my undergraduate advisor, Ellen Cowan, for sparking my scientific curiosity and giving me the confidence to pursue it.

It would be wrong to leave out my cat, Louie, for his contributions.

Table of Contents IV

Section	Page
1. Introduction	1
2. Literature Review	3
2.1 The North American and Coastal Ocean Carbon Budget	3
2.2 Seasonality in North American Carbon Fluxes	5
2.3 The Orbiting Carbon Observatory 2 (OCO-2)	6
2.4 XCO_2 Relationship with Surface CO_2 Fluxes	7
2.5 Geographic Characteristics of Mean XCO_2 Distribution	8
2.6 Temporal Scales of XCO_2 Variability	9
3. Research Questions	11
4. Methods	12
5. Results and Discussion	16
5.1 Linearly Detrended XCO_2 Spatial Means	16
5.2 XCO_2 Seasonal Cycle Amplitudes	19
5.3 Synoptic XCO_2 Anomaly Variability	22
5.4 Seasonality of XCO_2 Synoptic Anomaly Variability…	28
5.5 Synoptic XCO_2 Anomaly Skewness…	33
5.6 Summary of XCO_2 Statistical Parameters	34
5.7 Glint Mode Only Analysis…	39
5.8 Impact of Small-Scale Spatial Correlation	42
6. Summary	42
7. Conclusions and Future Directions	45
8. References	48

1. Introduction

Constraining surface CO_2 fluxes is a primary and ongoing pursuit in carbon cycle science, and a critical aspect of Earth system modeling, carbon monitoring, and mitigation activities. Atmospheric inversion studies that aim to accurately and robustly quantify surface CO_2 fluxes require descriptions of transport, mixing, and atmospheric CO_2 variations (Baker et al., 2006). While CO_2 variability is more well-documented near the surface than in the total air column, the introduction of satellite CO_2 observations is rapidly expanding column data and our understanding of its variations (Eldering et al., 2017). Total column-averaged CO_2 measurements are less sensitive to boundary layer vertical mixing and exchange with the free troposphere than surface CO_2 data and thus provide a novel constraint in surface CO_2 flux estimation (Keppel-Aleks et al., 2011).

Differences between CO_2 in continental and marine air have been observed and quantified by surface measurement networks. CO_2 in remote marine air has a well-mixed, hemisphere-mean signature while continental CO_2 is generally more variable due to the influence of regional human and terrestrial biospheric emissions (Geels et al., 2004). The impact of this land-ocean contrast in CO_2 behavior throughout the total atmospheric column is currently underexamined, as global coverage of total column CO_2 has only been made recently available with satellite data. Describing the continental CO_2 influence over the ocean is necessary to further constrain and interpret CO_2 fluxes. A recent study found transported urban CO_2 emissions had a significant impact on nearshore air-sea gas exchange over Monterey Bay, CA (Northcott et al, 2019), uncovering a mechanism that is not adequately accounted for in coastal carbon flux estimation. There is good agreement between different estimates of global and long-term mean ocean fluxes, but

temporal and spatial variability in CO_2, especially above coastal oceans, remains a major source of disagreement (Sitch et al., 2015).

New, high resolution satellite data can improve the understanding of atmospheric CO_2 variations. NASA's Orbiting Carbon Observatory 2 (OCO-2) provides global measurements of dry air mole fractions of total-column-averaged CO_2 in parts per million (XCO_2) (Eldering et al., 2017). Because carbon fluxes are so spatially and temporally heterogeneous, they need to be characterized at regional and sub-annual scales to monitor the effectiveness of different carbon sinks over time. XCO_2 data fills a gap in the spatially-sparse but temporally-dense land and ocean surface network measurements currently employed to resolve the carbon budget. Using OCO-2 XCO_2, we investigate spatiotemporal patterns in atmospheric CO_2 variability with a focus on land-ocean boundaries to better understand the transition between continental air mass XCO_2 and background maritime air mass XCO_2. We provide a characterization of spatial means, seasonal and sub-seasonal variability in XCO_2 across the conterminous U.S. and adjacent oceans, along with a comparison of land and ocean XCO_2 distributions along the east and west coastlines. We discuss how further work can attribute the observed variability to real signals either from surface fluxes or atmospheric transport and residual bias in OCO-2 soundings. We validate our results using XCO_2 from the Total Carbon Column Observing Network (TCCON), a ground-based network of Fourier transform spectrometers which have been used to investigate variability in column CO_2 (Keppel-Aleks et al., 2012). Attributing variability in XCO_2 can improve earth system modeling

and satellite measurement techniques as well as identify measurement biases over land and ocean (Baker et al., 2010).

2. Literature Review

2.1 The North American and Coastal Ocean Carbon Budget

Synthesis estimates show that North America is a net source of CO_2, contributing approximately ~1,008 teragrams of carbon (Tg C) to the atmosphere annually (Hayes et al., 2018). North American annual fossil fuel emissions are relatively well constrained to ~1,774 Tg C annually (Marcotullio et al., 2018). North American natural land and ocean sinks are estimated to offset its fossil emissions by ~43% with medium confidence (Hayes et al., 2018). Flux estimates of natural carbon sinks and sources have significant and variable uncertainty due to measurement gaps and disagreement among model representations of atmospheric transport and ecosystem carbon dynamics. Using inventory based, bottom-up approaches, the average annual uptake from 2004-2014 by the continental North American carbon sink and its coastal oceans was estimated as ~606 Tg C and ~160 Tg C, respectively (Hayes et al., 2018). Coastal oceans are affected by direct air-sea gas exchange as well as transport of dissolved organic and inorganic carbon from inland waters (Fennel et al., 2019). Limited observations and complex small-scale variability create significant uncertainty in coastal ocean carbon flux estimates. To predict the strength of these sinks into the future and assess

economic/ecologic risks such as coastal acidification, temporal and spatial variations in CO_2 flux must be further constrained (Fennel et al., 2019).

While the Atlantic coastal ocean acts a net carbon sink, it has a large-scale meridional gradient in air-sea CO_2 flux, with more carbon uptake in the northern latitudes (Fennel et al., 2019). To the North of Cape Hatteras, there is a prominent seasonal cycle in CO_2 flux. Cool temperatures increase CO_2 solubility and spur uptake in the winter. CO_2 uptake through photosynthesis continues through spring, while summer and fall are periods of outgassing due to warming and respiration. To the South of Cape Hatteras, biological CO_2 uptake is reduced and there is less seasonality in CO_2 flux. In this region, there are sporadic drawdown events due to input from high-nutrient Gulf Stream water and riverine inputs (Fennel et al., 2019).

The Pacific coastal ocean is acted upon by westerly winds, which cause equatorward currents and upwelling of carbon rich water (Fennel et al., 2019). Though this causes significant CO_2 outgassing in the region, the Pacific coast is still a weak to moderate net carbon sink. Similar to the Atlantic, there is stronger CO_2 flux seasonality in northern latitudes of the Pacific. The region has large spatial and temporal variability in carbon flux due to variable wind forcing, freshwater influence, rough bathymetry, and primary production. ENSO conditions drive interannually alternating periods of either dominant CO_2 efflux from upwelling and outgassing or CO_2 influx from relaxation and biological drawdown (Fennel et al., 2019). The dynamics of the coastal ocean off California is heavily controlled by wind-driven coastal upwelling, which Garcia-Reyes

and Largier (2012) divided into three seasons: April-June upwelling, July-September relaxation, and a December-February storm season.

2.2 Seasonality in North American Carbon Fluxes

For our study domain and the entire Northern Hemisphere, the seasonal CO_2 cycle is primarily driven by the biosphere. It can be characterized by a seasonal maximum CO_2 release (net respiration) and CO_2 uptake (net photosynthesis) controlled by plant growing seasons (Olsen and Randerson, 2003). XCO_2 seasonal minimum and maximum values are lagged by several months from peak CO_2 drawdown and release at the surface. The areas in our study domain with the highest gross primary productivity are along the western seaboard, the southeast, the northeast, and north of the Great Lakes (Zhang et al., 2017). Boreal forest carbon fluxes have especially large seasonal amplitudes due to the short length of the boreal growing season. Seasonality induced by the short boreal forest growing season and seasonal northern latitude human emissions result in high surface and column CO_2 seasonality in northern latitudes (Sweeney et al., 2015). Modeled global column CO_2 amplitudes were greatest over eastern Eurasia and eastern boreal North America. Compared to Europe, mean seasonality in human emissions is weak for the United States because a secondary summer peak due to air conditioning counteracts the wintertime heating peak, and wintertime heating demands are weakening with interannual temperature rise (Sweeney et al., 2015). Anthropogenic emissions are greatest along the densely populated northeastern coast and greater in general over the eastern half of North America (Marcotullio, 2018).

2.3 The Orbiting Carbon Observatory 2 (OCO-2)

NASA's Orbiting Carbon Observatory 2 provides global coverage of XCO_2 with a ground track that repeats every 16 days and eight footprints across track (Eldering et al., 2017). XCO_2 is the average concentration of CO_2 in a column of dry air extending from the Earth's surface to the top of the atmosphere. OCO-2 retrieves XCO_2 from NIR spectra (1.61 and 2.06 μm) of passive solar radiation reflected/scattered back from the surface (land, ice or water) and offers a fine spatial resolution (~1.29 x 2.25 km) and precision (0.5 ppm) (Chatterjee et al., 2017). The ratios of column-averaged CO_2 and O2 number densities are taken along the optical path between the Sun, surface footprint, and instrument, and multiplied by the concentration of column-averaged oxygen to estimate XCO_2. OCO-2 provides retrievals from both nadir pointing mode and glint pointing mode, the latter increasing signal and reducing retrieval uncertainties over the ocean (Baker et al., 2010). The Level 2 V9 data product we use provides geolocated XCO_2 from cloud-free scenes along with retrievals of surface pressure, albedo, aerosol content, water vapor, and temperature profiles. Because retrieval is sometimes inhibited by clouds, thick aerosols, and topography inhomogeneities, the data products contain error measures for quality filtering.

These new XCO_2 measurements can improve carbon flux estimates produced by atmospheric inverse models, which have difficulties representing atmospheric vertical mixing. They improve upon the existing in situ measurement network by providing global coverage and upon CO_2 observations from the GOSAT satellite, which uses measurements of atmosphere CO_2 thermal NIR emissions, by providing more frequent

soundings, lower retrieval errors, and a smaller field of vision. OCO-2 enables top-down carbon flux estimation at finer regional scales than could previously be achieved. OCO-2 data is validated using XCO_2 from the Total Carbon Column Observing Network (TCCON), which has 23 operational instruments worldwide and three within our North American study domain. TCCON XCO_2 is collected with upward looking, ground-based spectrometers that measure trace gas absorption in the solar spectrum. The primary science mission of OCO-2 is to characterize and monitor the geographic distribution of CO_2 sinks and sources over time, as they control the atmospheric CO_2 concentration and therefore regulate our climate.

2.4 XCO_2 Relationship with Surface CO_2 Fluxes

Ongoing efforts aim to constrain the impact of surface fluxes and different atmospheric transport mechanisms on XCO_2 patterns. XCO_2 measurements have a large footprint, as the area of surface flux influencing the column increases with altitude, giving XCO_2 its unique ability to capture large-scale carbon gradients and provide information about continental-scale sinks and sources (Baker et al., 2010; Olsen and Randerson, 2003). It can also be used to infer regional surface fluxes when paired with top-down atmospheric inversion methods (Keppel-Aleks et al., 2011; Baker et al., 2006). While the signal of large-scale variability is larger than the signal of regional fluxes in XCO_2, they can be drawn out if the biospheric CO_2 mean state is accurately described (Keppel-Aleks et al., 2011).

Total column-averaged CO_2 measurements are affected by different gradients and modes of variability than CO_2 at the surface. A study by Olsen and Randerson (2003) investigated differences in surface and column CO_2 using an atmospheric transport model simulation. Because column CO_2 includes a larger fraction of the atmosphere than surface layer CO_2, variability driven by surface fluxes creates a bigger change in concentration at the surface. In general, column CO_2 was less variable spatially and temporally than surface CO_2 and diurnal variability contributed less to overall variability in the column than from processes that take place over multiple days. High frequency variability driven by diurnal surface fluxes decreased with altitude in the modeled column. Seasonal variability in column CO_2 is more similar to surface CO_2, though there are phase delays in the timing of maximum and minimum seasonal peaks in the column, likely due to the time required for vertical mixing. Compared to surface CO_2 in the Northern Hemisphere, column-averaged CO_2 is greater in the summer and fall and lower in the winter and spring. The seasonal cycle of surface CO_2 had a much higher amplitude over land than ocean, whereas land and ocean seasonality in the column were more similar. The spatial north-south gradient in surface CO_2 during the growing season was also more pronounced over land than ocean compared to column CO_2. They speculated that the lower contrast between land and ocean XCO_2 was likely due to more wind dispersal in the free troposphere than in the boundary layer (Olsen and Randerson, 2003).

2.5 Geographic Characteristics of Mean XCO_2 Distribution

The geographic variation in XCO_2 means reflects a combination of surface carbon fluxes and large-scale atmospheric transport including mean meridional circulation,

stationary eddies, and transient eddies (Crisp et al., 2011; Parazoo et al., 2011). XCO_2 has primarily meridional patterns that vary over the seasonal cycle, with larger variations in the north-south direction than the east-west direction. Due to its latitudinal structure, global patterns are commonly assessed using zonal means (Crisp et al., 2011). During the winter and spring, biospheric and anthropogenic CO_2 emissions decrease from north to south, creating a decreasing north-south gradient in XCO_2 (Keppel-Aleks et al., 2011). During the growing season, transition from net respiration to net photosynthetic uptake reverses the winter/spring gradient and creates a relatively stronger increasing north-south gradient in XCO_2 (Keppel-Aleks et al., 2011). Zonal mean estimates of XCO_2 from GOSAT and OCO-2 show that XCO_2 decreases with latitude from 30 N to 50 N from June to August, primarily reflecting the strong growing season gradient after averaging over a full annual cycle (Liang et al., 2017).

2.6 Temporal Scales of XCO_2 Variability

As discussed in the previous sections, the biosphere creates a prominent seasonal cycle in both XCO_2 and surface CO_2, though XCO_2 is more affected by transported seasonal variability in addition to local surface flux seasonality. Keppel-Aleks et al. (2011) analyzed TCCON data to study the imprint of surface fluxes and horizontal atmospheric transport on XCO_2 variability. They found XCO_2 was more sensitive to the advection of large gradients by synoptic-scale weather than local surface fluxes and local vertical mixing. Synoptic-scale XCO_2 variations, primarily driven by transient eddy

advection across the north-south meridional gradient, contributed up to half the seasonal XCO_2 cycle in mid-latitude TCCON observations. Robust spatiotemporal descriptions of the mean meridional gradients in CO_2 are therefore necessary for CO_2 flux attribution, with significant impacts on estimates of the net annual North American sink (Keppel-Aleks et al., 2011). Synoptic-scale variations occur on time scales of 1-2 weeks and spatial scales of ~1000 km. Large-scale transient eddies are primarily driven by baroclinic instability and the net effect of their transport can be evaluated by monthly averaging (Parazoo et al., 2011). Over multiple synoptic cycles, Parazoo et al., (2011) found net poleward transient eddy transport, with poleward transport of CO_2 greater than fossil CO_2 emissions in mid-latitudes. This effect causes reduced seasonality in mid-latitudes and amplify seasonality at high latitudes (Parazoo et al., 2011).

Torres et al. (2019) continued resolving the variance budget of XCO_2 using TCCON and OCO-2 data. Variability from synoptic-scale transport was twice as large in magnitude as the variability induced by local diurnal fluxes in OCO-2 XCO_2 (Torres et al., 2019). Mesoscale variability, induced by advection from small-scale weather features, was about half the size of the diurnal variability during the growing season, but greater than diurnal variability in the winter. Synoptic variability in TCCON and OCO-2 XCO_2 were strongly correlated to the magnitude and seasonal cycle of the large-scale north-south gradient, while mesoscale variability only exhibited a moderate correlation. Advection of variations by mean wind and variability produced by transient eddies acting on the mean gradient are the drivers of explained synoptic OCO-2 XCO_2 variability (~0.5 ppm). Unexplained variability caused by errors and spatially-coherent retrieval bias is on

the same order (0.3 to 0.8 ppm), overprinting real variability and affecting the independence of along-track observations. Compared to land XCO_2, this variability is about half the size in ocean XCO_2, which is less complicated by topography and albedo retrieval problems (Torres et al., 2019).

3. Research Questions

Based on the importance of understanding spatiotemporal variations in XCO_2 described above, my research is focused on the following science questions:

- From the open ocean, across the coast, into the continental interior, how do properties of atmospheric XCO_2 (central tendency, seasonal and synoptic variability, synoptic anomaly seasonality) vary in space and time?
- How do these patterns compare over different latitudes of the east and west continental U.S. coasts and between land and ocean XCO_2 populations?
- Assuming that a continental signal can be identified, how far does it extend over the coastal ocean and into the open ocean before transitioning to a well-mixed marine air signal? Does this boundary region differ from east to west coast in its extent?
- How do our results differ when using retrievals from combined nadir and glint pointing modes versus glint mode only?
- To what degree is the analysis impacted by small-scale spatial correlation in OCO-2 XCO_2 discussed in Torres et al (2019)?

4. Methods

We analyze XCO_2 patterns using combined glint and nadir mode NASA Orbiting Carbon Observatory- 2 (OCO-2) column-averaged dry air mole fraction CO_2 (XCO_2) data retrieved from 9/6/2014 to 6/1/2019. We use the V9r OCO-2 Level 2 data product of bias-corrected XCO_2 retrieved using the Atmospheric CO_2 Observations from Space (ACOS) algorithm (O'Dell et al., 2018). August 2017 is omitted due to on-orbit calibration of the satellite.

The first analysis will be conducted on 20 latitude bands of cross-coast XCO_2 observations from 30 N – 50 N and -145 W to - 50 W, across the conterminous United States and adjacent ocean basins (Figures 1a, 2a, 3a, & 4a). The study domain is evaluated zonally due to the dominant west to east wind direction and dominant mean structure of XCO_2 (Tables 1-4). Longitudinal patterns are also assessed by dividing each latitude band into bins of 5 degrees longitude. Averaging XCO_2 parameters according to this grid ensures adequate data coverage for a full seasonal cycle, given gaps in data coverage due to OCO-2's sparse 16-day repeat cycle and to cloud cover. A seasonal data coverage bias remains in some northern latitude bins and its impact is discussed in Section 4.

A second analysis will focus on comparing onshore to offshore XCO_2 distributions by aligning bins with the east and west coastlines (Figures 1b-c, 2b-c, 3b-c, and 4b-c). The midpoint of the coastline for a given latitude band is identified, dividing four offshore bins from four onshore bins (each bin spanning 1 degree latitude x 5

degrees longitude), allowing for the comparison of bins far enough inland and far enough offshore to see a transitions in XCO_2 behavior relating to land-ocean transport patterns, fluxes, or retrieval biases.

The procedure for each analysis is described below:

1. Filter out poor quality XCO_2 soundings by excluding all soundings flagged with a "1" for poor data quality in the quality flag variable in V9 Lite files. This quality filter identifies thresholds for different variables that correlate with significant XCO_2 bias or scatter. Combined glint and nadir XCO_2 observations used in the "original" analysis are denoted as X. Glint mode only XCO_2 observations used in the following "glint only" analysis are denoted as $_{glint}X$.

2. Detrend data using a linear regression on an XCO_2 time series encompassing the full study domain. This strong and direct trend (R = 0.8) describes a long-term linear increase in XCO_2, reflecting the long-term increase in anthropogenic CO_2 emissions. For the computed trend, the intercept uncertainty is 0.3 years, the slope uncertainty is $1.5 * 10^{-4}$ ppm/ year, and the covariance is $-4.7 * 10^{-5}$ ppm/year.

Eq. 1

$$\hat{X}\ (ppm) = (time\ in\ decimal\ years * 2.6) - 50$$

3. Compute long-term temporally detrended anomalies, X', by removing values predicted by the long-term linear trend in XCO_2 all observations.

Eq. 2

$$X' = X - \hat{X}$$

4. For each bin, compute its mean over all years of long-term temporally detrended data, $\overline{X}$. This is done to remove the spatial mean pattern in the data for a better direct comparison of seasonal and synoptic variability between bins. Compute long-scale temporally and spatially detrended anomalies, X''.

Eq. 3

$$X'' = X' - \overline{X}$$

5. For each bin, compute the monthly means and standard deviations of large-scale temporally and spatially detrended anomalies. Using the monthly averages of the anomalies, construct the mean seasonal cycle of each bin. Compute each bin's seasonal amplitude, A, by subtracting the minimum monthly average value from the maximum monthly average value of the mean seasonal cycle.

Eq. 4

$$\vec{X} = monthly\ averages\ of\ X''$$

$$A = \vec{X}\,max - \vec{X}\,min$$

6. Calculate monthly deseasonalized anomalies, X^*, by subtracting the monthly average values for the corresponding month of large-scale temporally and spatially detrended anomalies. After removing the mean seasonal cycle, the data primarily reflects

synoptic variability. Compute the average X^* standard deviation, variance, skewness, kurtosis, and the month of peak X^* variance for each bin.

Eq. 5

$$X^* = X'' - \vec{X}$$

We then repeat the analysis using only glint mode data, ${}_{glint}X$, compare variance ratios between the glint mode analysis and original combined mode analysis, X, and record the degree to which the variance changes between the two. This is done to evaluate whether the original analysis results are robust or if they are sensitive to viewing mode.

We investigate small-scale spatial correlation identified by Torres et al. (2019) by averaging combined glint and nadir retrievals into 0.1 degree latitude bins along the orbit track. This averaging scale is consistent with scale of spatial correlation in XCO_2 found in Torres et al., (2019). We repeat the analysis using the orbit-averaged data, ${}_{orbit}X$ and compare the ratio of variance from the orbit-averaged analysis to the original analysis for each bin. This is done to evaluate whether the variance observed in our original analyses are robust to the impact of instrument and algorithm noise as well as small spatial-scale geophysical signals.

5. Results and Discussion

5.1 Linearly Detrended XCO_2 Spatial Means

The geographic variation observed in atmospheric XCO_2 reflects a combination of surface carbon fluxes and large-scale atmospheric circulation, and the relative influence of these mechanisms vary across the study domain. A spatial map of detrended XCO_2 spatial means across the full study domain is computed using Equation 2 and displayed in Figure 1a. Figures 1b and 1c are computed in the same manner using spatial bins that are aligned with the land-ocean boundary along the west and east U.S. coastlines to highlight differences between land and ocean XCO_2 distributions. Southern bins are defined as bins between 30 N and 40 N. For the west coast, northern bins are defined as bins between 40 N and 50 N. Because Figures 1b and 1c are meant to illustrate land-ocean differences, northern bins for the east coast are defined between 40 N and 45 N, as bins cannot be adequately aligned with coastline above 45 N.

Figure 1 shows large scale geographic variation in XCO_2 annual means with latitude. Annual mean XCO_2 decreases from 30 N to 50 N, consistent with findings in Liang et al., (2017). The average mean XCO_2 for northern (40-50 N) and southern (30-40 N) is -0.8 ppm and -0.1 ppm respectively. The average mean XCO_2 for the Pacific Ocean is slightly more positive than that of the continent and Atlantic Ocean. The net XCO_2 mean is slightly negative, in contrast with the surface CO_2 budget, in which fossil fuel emissions cause North America to be a net source of CO_2 to the atmosphere (Hayes et al., 2018). This indicates that mean XCO_2 patterns primarily reflect mean east-west

atmospheric transport as opposed to local surface carbon fluxes. A seasonal sampling bias occurs in ocean bins and some near-coast land bins above ~43 N, where there are few observations in January and December. This bias causes an incomplete picture of the seasonal cycle and a lack of representation of the greater wintertime emissions in certain northern bins. This could exaggerate the north-south gradient we observe in spatial XCO_2 means.

For both Figures 1b and 1c, there is not a clear contrast between adjacent land and ocean bin means, highlighting the importance of horizontal atmospheric winds smoothing east-west variations. For both the west and east coasts (Figures 1b and 1c), spatial means are more positive in the southern bins than northern bins, though the north-south difference is greater for the east coast. The north-south difference is greater for land bins than ocean bins over the west coast (1.06 ppm vs. 0.60 ppm). The north-south difference is more similar for land and ocean bins over the east coast (1.16 ppm vs 0.97 ppm). Surface carbon fluxes also have a greater north-south difference over land due to growing season carbon uptake by the terrestrial biosphere, though unlike what we see in XCO_2, this difference is more prevalent over the eastern United States at the surface due to the region's higher primary productivity. For the west coast, the average spatial mean of all land bins is more negative than the average of ocean bins (-0.37 ppm vs -0.05 ppm). In contrast, the average spatial mean of all ocean bins is more negative than the average of land bins (-0.36 ppm vs. 0.17 ppm) for the east coast. More negative ocean means over the Atlantic could indicate that airmasses off the east coast have integrated the full

continental terrestrial drawdown, accentuated by the sampling bias by overweighting the summertime data.

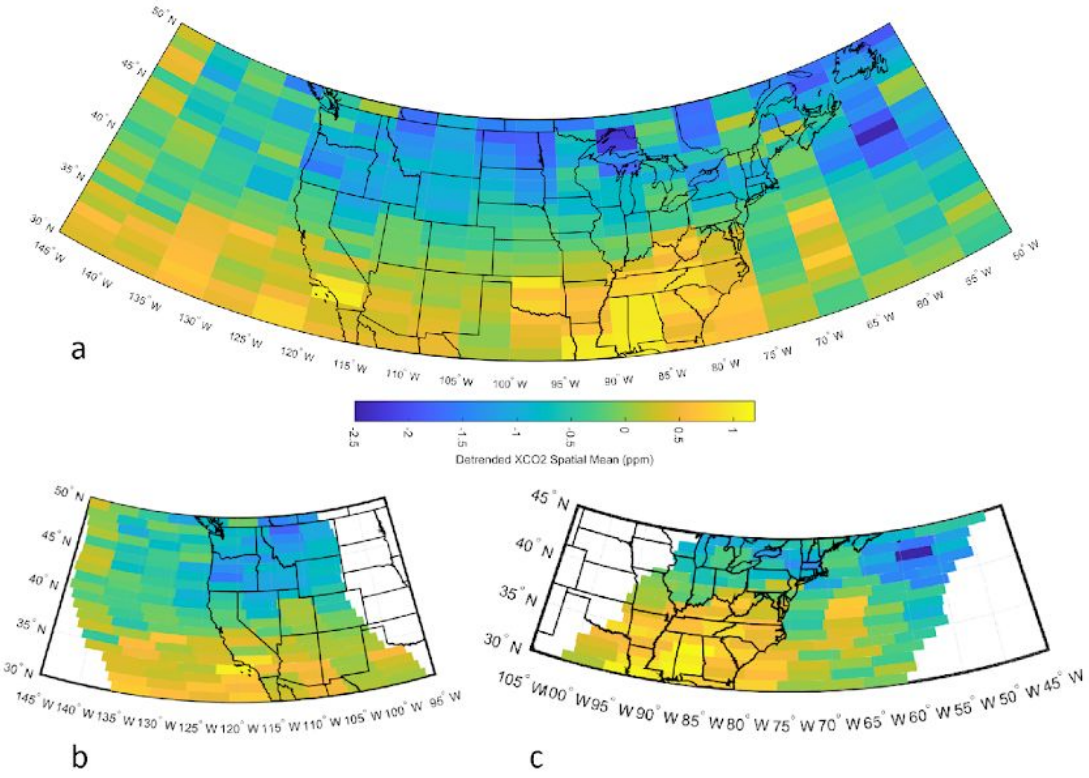

Figure 1. Figure 1a is a spatial map of the time-mean detrended XCO_2 for 1x5 degree latitude-longitude grid cells. Figure 1b is a spatial map of the time-mean detrended XCO_2 for grid cells that are aligned with the western United States coastline into 4 ocean bins and 4 land bins for each latitudinal band. Figure 1c is a spatial map of the time-mean detrended XCO_2 for grid cells that are aligned with the eastern United States coastline into 4 ocean bins and 4 land bins for each latitudinal band.

5.2 XCO_2 Seasonal Cycle Amplitudes

The seasonal variability observed in XCO_2 could reflect seasonality in local carbon fluxes or transported variability from regions upstream in the mean atmospheric transport path. From our findings in the spatial patterns of XCO_2 means, we would expect transported variability to be an important component in XCO_2 seasonal variability. If seasonality in local carbon fluxes are contributing to the seasonal amplitudes we observe in XCO_2, XCO_2 amplitudes would be increased over regions with the most biosphere productivity, where surface CO_2 uptake and release rates would be higher in the summer and winter, respectively.

A spatial map of XCO_2 seasonal amplitudes across the full study domain is computed using Equations 3 and 4 and displayed in Figure 2a. Figures 2b and 2c are computed in the same manner using spatial bins that are aligned along the west and east U.S. coastlines. Northern bins for Figure 2b are defined between 40 N and 50 N, and defined between 40 N and 45 N for Figure 2c. Southern bins are defined between 30 N and 40 N for Figures 2b and 2c. Seasonal amplitudes are highest over the continental northeast and adjacent Atlantic Ocean, and lowest over the western half of the continent. Bins between 125 W and 100 W (western half of continent) have an average amplitude of 6.3 ppm, which is almost 2 ppm lower than the average for the rest of the domain (8.2 ppm).

The continental patterns are consistent with the seasonality in underlying surface CO_2 fluxes, which are more seasonal for the more vegetated eastern United States.

Seasonal amplitudes are greater to the north of Cape Hatteras in the Atlantic Ocean, consistent with descriptions of air-sea flux in Fennel et al., (2019). However, greater seasonal amplitudes over the northern Pacific Ocean compared to the adjacent forested continent suggests XCO_2 amplitudes are not totally driven by local fluxes. The spatial pattern in amplitudes is similar to results found in a study by Sweeney et al. (2015), in which column CO_2 climatologies are compared to dominant wind transport patterns. The study found a continuous, mostly meridional band of elevated seasonal column CO_2 amplitudes. Upon reaching the west coast, it diverts in a northeast direction away from the U.S. northwest and toward British Columbia. The greater Pacific Ocean XCO_2 amplitudes shown in Figure 2 may, therefore, be a result of seasonal variations upwind being transported from Eurasia. The band dips slightly lower in latitude over eastern North America, where we see the greatest XCO_2 amplitudes. The signal of this highly seasonal boreal air seems to track over the Atlantic Ocean. Atlantic Ocean primary productivity is highly seasonal to the north of Cape Hatteras (Fennel et al., 2019), so this could also be contributing to the high seasonal XCO_2 amplitudes we observe there. Low seasonality air from southern latitudes are shown to blow upward toward the continental southwest, where Figure 2b shows the lowest XCO_2 amplitudes.

Over the oceans, seasonal amplitudes gradually decrease from north to south while seasonal amplitudes over land vary more with longitude. The west coast exhibits significant differences between land and ocean populations. Figure 2b shows a clear contrast across the land-ocean boundary in the northern latitudes. West coast ocean bins have a greater average seasonal amplitude than land bins (8.1 ppm vs. 6.3 ppm) and the

difference between northern and southern bins is more pronounced for ocean bins than land bins. For the east coast, land and ocean bins have more similar average amplitudes (7.9 ppm vs. 7.8 ppm) and more similar north-south difference. Land and ocean similarities for the east signify that the east coast more closely reflects North American seasonal carbon cycling while the west coast seasonal XCO_2 cycle is likely more influenced by transported variability from other continents.

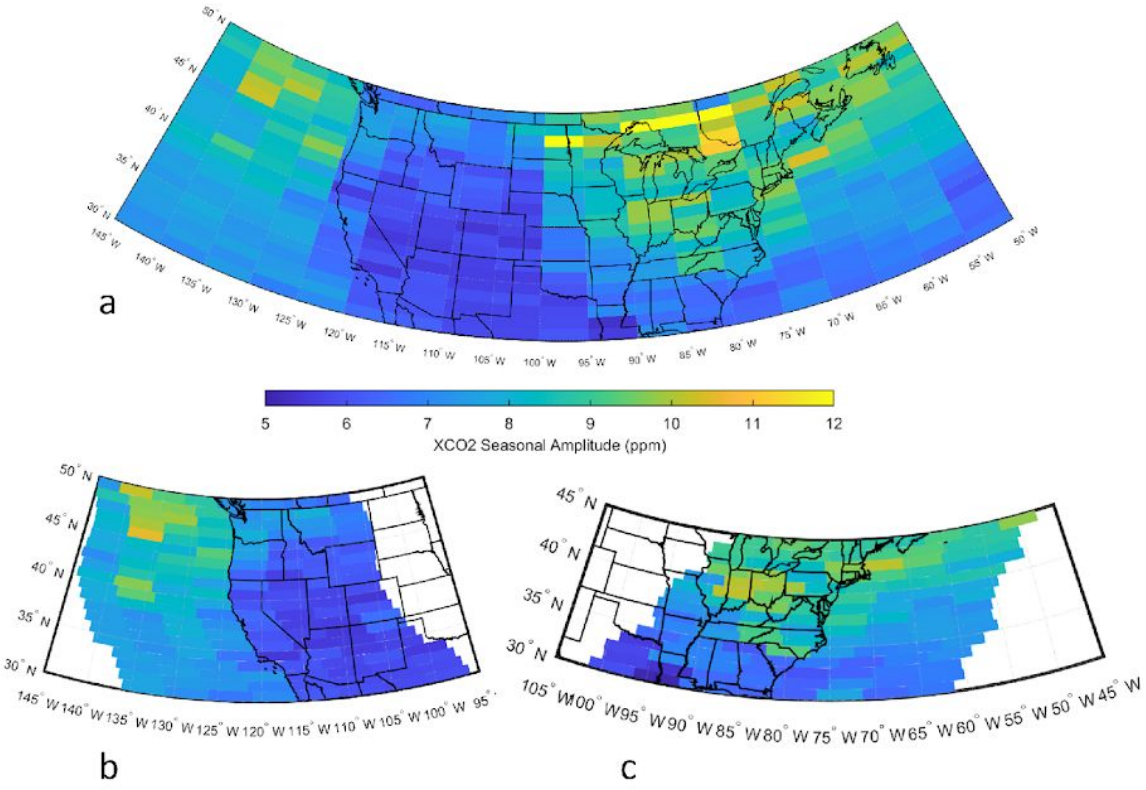

Figure 2. Figure 2a is a spatial map of XCO_2 seasonal amplitudes for 1x5 degree latitude-longitude grid cells. Figure 2b is a spatial map of XCO_2 seasonal amplitudes for grid cells that are aligned with the western United States coastline into 4 ocean bins and 4 land bins for each latitudinal band. Figure 2c is a spatial map of the XCO_2 seasonal amplitudes for grid cells that are aligned with the eastern United States coastline into 4 ocean bins and 4 land bins for each latitudinal band.

5.3 Synoptic XCO_2 Anomaly Variability

As indicated in the previous sections, variations in spatial XCO_2 means and seasonal amplitudes are shaped by large-scale flux and transport patterns. Smaller scale

advection and stirring of these large-scale spatial gradients, namely the north-south growing season gradient, are the primary driver of temporal synoptic-scale variability in XCO_2 (Keppel-Aleks et al., 2011). After linear detrending, spatial detrending, and seasonal detrending, variability in the resulting XCO_2 anomalies primarily reflect variability on the atmosphere mesoscale (on the order of 10s to ~100 km and hours to days) and synoptic-scale (on the order of 100s to ~1000 km and days to a couple of weeks). Though our current methods aggregate mesoscale/synoptic and subseasonal/interannual variability, later efforts will focus on partitioning the two, and for simplicity here the seasonally detrended anomalies are referred to as synoptic anomalies.

A spatial map of synoptic-scale XCO_2 anomaly variability across the full study domain is computed using Equation 5 and shown in Figure 3a. Figures 3b and 3c are computed in the same manner using spatial bins that are aligned along the west and east U.S. coastlines to highlight differences between land and ocean XCO_2 populations. Northern bins for Figure 3b are defined between 40 N and 50 N, and defined between 40 N and 45 N for Figure 3c. Southern bins are defined between 30 N and 40 N for Figures 3b and 3c. Synoptic variability is greatest above the continental northwest and northeast (2-3 ppm^2) and greater for land bins than ocean bins, similar to the findings in Torres et al (2019). Variability over the ocean basins is more spatially coherent, while the spatial patterns in variability over land vary more with latitude and longitude.

Distinct meridional and land-ocean patterns are present in synoptic XCO_2 variability. For bins following the west coast (Figure 3b), there is a clear contrast in

synoptic XCO_2 anomaly variance for adjacent land and ocean bins, resembling the contrast we observe in seasonal amplitudes. There is a cluster of high variance bins above the Rocky Mountains in Idaho and western Montana, containing the highest variance bin for the entire domain. Variance is also higher over northern Colorado and above Los Angeles than surrounding bins. Overall, northern bins have a higher average variance (1.8 ppm^2) than the average variance of southern bins (1.2 ppm^2). For the west coast, average variance of all land bins is almost double the average variance of ocean bins (1.9 ppm^2 vs. 1.0 ppm^2) and land bins have a greater north-south difference.

For bins following the east coast (Figure 3c), synoptic XCO_2 variability is greatest over upstate New York, Vermont, New Hampshire, and Maine. Compared to the west coast, there is a less clear contrast in variability for adjacent land and ocean bins. The average variance of all land bins is slightly higher than that of ocean bins (1.6 ppm^2 vs. 1.1 ppm^2) and the north-south difference is similar for land and ocean bins. Compared to the northwest coast, there seems to be more east-west smoothing of XCO_2 across the east coast, as observed in the seasonal amplitudes. There is a continental signal to the synoptic variance that tracks out over the northern Atlantic.

The patterns seen in Figure 3 could have several possible explanations, the first being patterns of atmospheric transport. Advection of variations by mean winds and variability produced by transient eddies acting on the mean spatial XCO_2 gradient create synoptic variance in XCO_2 (Keppel-Aleks et al., 2011). With this in mind, we would expect XCO_2 variance to be greatest in the summer in areas that experience the most atmospheric mixing of northern air with low mean XCO_2 and southern winds with high

mean XCO_2. When the north-south gradient reverses after the growing season, we would also expect advection to produce synoptic XCO_2 variability in regions where southern air with low mean XCO_2 mixes with northern air with high mean XCO_2, though this gradient is weaker. The relative strength of the two gradients differs by region due to spatial emissions patterns and large-scale transport. Mean synoptic weather development in North America is greatest over coastal British Columbia and Arizona and most prevalent during the cool season, though synoptic weather peaks in April for most of the inland continent (Lareau and Horel, 2011). Synoptic XCO_2 variability is low over Arizona because synoptic weather needs to be acting on a spatial gradient, and the winter gradient is weak compared to the summer gradient, as shown in Figure 1. In section 5, we discuss seasonality in synoptic XCO_2 variability and the relative impact of seasonal XCO_2 gradients.

Spatiotemporal variations in ecosystem and anthropogenic surface fluxes, though generally obscured by large-scale XCO_2 variations, can induce synoptic variability in XCO_2 (Keppel-Aleks et al., 2011). During the growing season, local diurnal fluxes were found to contribute up to 1-2 ppm of within-day XCO_2 variability at midlatitude TCCON sites (Torres et al., 2019). It is possible that areas with high synoptic XCO_2 variability could be a result of surface ecosystem fluxes responding to synoptic weather driven temperature and precipitation changes. In future analysis, we can use band pass filtering to further parse temporal scales of variability and isolate the local flux signal, which unlike weather events, is tied to a diurnal cycle (Torres et al., 2019). The high variance

bin over Los Angeles could be tied to the advection of dense local anthropogenic fluxes in the boundary layer, trapped to the west of the Sierra Nevada range.

We see similarities and differences in the observed synoptic XCO_2 variability and synoptic XCO_2 variability simulated by GEOS-5, a supercomputer model of atmospheric CO_2 levels. The model shows CO_2 stirring by large-scale weather patterns over a year (Jing et al., 2018), with the highest concentrations over major emissions sources, namely eastern North America, Europe, and Asia. Regions that exhibit the most synoptic variability in the simulation are similar to those observed in the synoptic XCO_2 anomalies, with the exception of elevated synoptic XCO_2 variance over the Pacific Northwest. In the simulation, less large-scale eddies act on this region relative to the ocean and the eastern United States over the course of a year.

High synoptic OCO-2 XCO_2 variability over the western United States appears to have a spatial correlation with topography, with greater variability over mountain ranges such as the Sierra Nevada-Cascades and the Rockies compared to the plateaus/basins down their eastern slope, such as the Nevada Basin, eastern Colorado, and eastern Montana. Mountain-related meteorology could induce more mixing in these regions, compounded by variability in biospheric fluxes with elevation. This could be why variability is not heightened over lower elevation ranges like the Appalachians that do not generally reach the treeline. Additionally, there is a potential topography-related bias in OCO-2 retrievals due to errors in the prior surface pressure (Kiel et al., 2019). Offsets in the geolocation of the pointing of the spectrometer cause significant errors in assumed surface pressure above rough topography (Kiel et al., 2019). Over Lauder, New Zealand,

the variance induced by this error was 0.55 ppm^2 in v9 OCO-2 XCO_2 data (Kiel et al., 2019). In the synoptic XCO_2 anomalies shown in Figures 3a and 3b, changes in variance that could correspond to topographic differences between bins are at or above 1 ppm^2, which suggests the topographic effect may not entirely reflect an instrument bias.

In addition to the advection of large XCO_2 gradients, the effects of topography, and local flux variability, it is also possible that patterns of synoptic variability are caused by retrieval issues. Identifying and correcting the biases produced by aerosols, cloud cover, and albedo is an ongoing pursuit of the OCO team. The synoptic XCO_2 anomaly variances presented in Figures 3a-c are heightened over the northwest and northeast, which are prone to cloudiness. Massie et al., (2017) estimated variance produced by cloud bias between 1.4 and 6.8 ppm^2. The higher variance XCO_2 is likely not related to cloud bias because variance is generally highest in the summer for those regions, whereas we would expect peak cloudiness in the winter (Stubenrauch et al., 2010). We discuss this and other seasonal differences in synoptic XCO_2 variability in the section below.

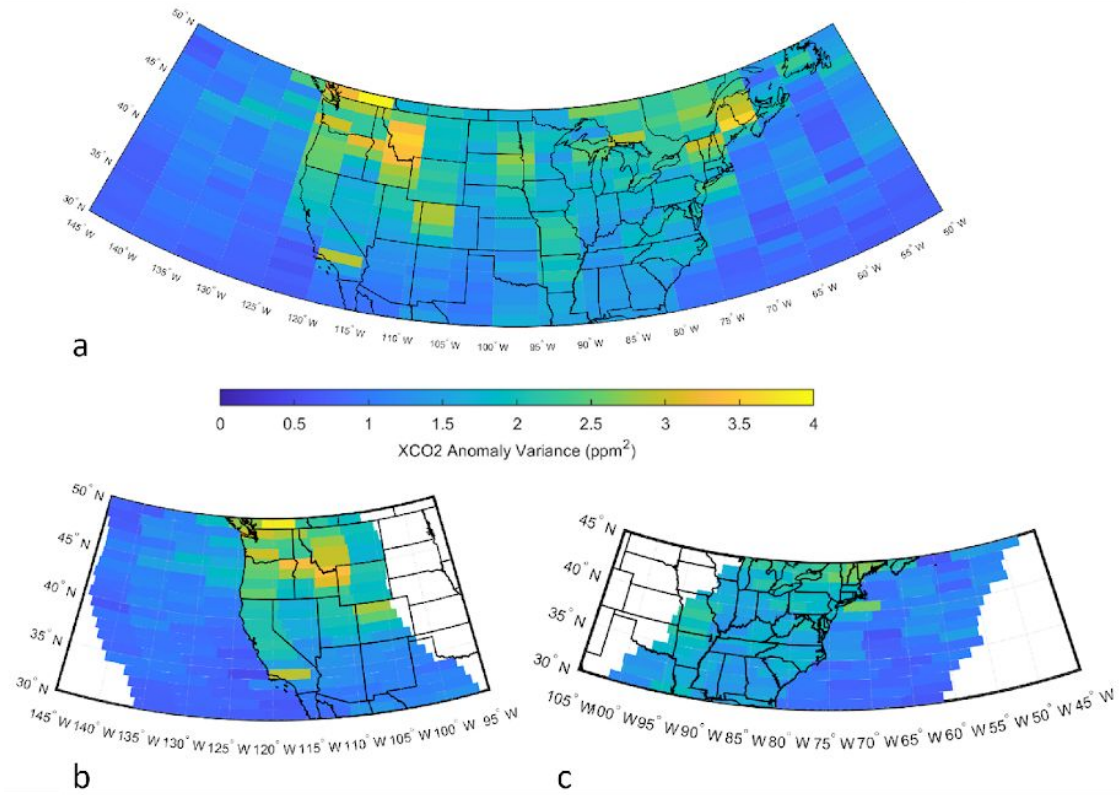

Figure 3. Figure 3a is a spatial map of synoptic XCO_2 anomaly variance for 1x5 degree latitude-longitude grid cells. Figure 3b is a spatial map of synoptic XCO_2 anomaly variance for grid cells that are aligned with the western United States coastline into 4 ocean bins and 4 land bins for each latitudinal band. Figure 3c is a spatial map of synoptic XCO_2 anomaly variance for grid cells that are aligned with the eastern United States coastline into 4 ocean bins and 4 land bins for each latitudinal band.

5.4 Seasonality of XCO_2 Synoptic Anomaly Variability

Seasonal patterns in synoptic XCO_2 variability provide information about what processes are driving the spatial patterns in synoptic XCO_2 variability. Figure 4a is a

spatial map showing the months of peak synoptic XCO_2 variability across the full study domain. Figures 4b and 4c are computed in the same manner using spatial bins that are aligned along the west and east U.S. coastlines to highlight differences between land and ocean XCO_2 populations. Northern bins for the west coast (Figure 4b) are defined between 40 N and 50 N, and defined between 40 N and 45 N for the east coast (Figure 4c). Southern bins are defined between 30 N and 40 N for both coasts.

Figure 4 shows that most bins peak in July, consistent with findings in Keppel-Aleks et al., (2011) that synoptic XCO_2 variability is primarily driven by advection across the meridional growing season gradient. This signifies that advection-induced variations are a larger contributor to observed synoptic XCO_2 variability than retrieval covariates, especially over the midcontinent, where almost all bins peak in the summertime. Bins that exhibit the highest synoptic XCO_2 variability (the northwest and northeast shown in Figure 3) usually have peak variance in the summer months. The exception is a high variance bin over southern California, which peaks in October. Bins farther south and farther north from the middle of the mean gradient (shown in Figure 1 to be ~40 N) more often have peak variability outside of the growing season. This indicates that the mixing of XCO_2-elevated and XCO_2-depleted air during the growing season is not the primary driver of synoptic variability in those regions.

Most bins from 30 – 45 N and east of 125 W (the west coast) reach peak variability in June, July, and August. The spatial distribution of bins that peak in the summertime could indicate when there is the most advection of the summertime gradient and provide insight toward the phasing of biospheric fluxes. From 45-50 N, bins most

commonly peak in June. Chen and Yang (2020) observed an earlier start of the growing season above 43.5 N, and a delayed start of the growing season below in MODIS observations over the period 2001-2014. This could be related to the earlier XCO_2 synoptic anomaly peaks we see in the northern bins. In Figure 4b showing the west coast, a larger fraction of bins peak earlier in the growing season (June) compared to the western land bins. For the east coast (Figure 4c), bins that peak in June are mainly above 40 N. Synoptic XCO_2 variance peaking in June could be indicative of northern latitude boreal fluxes, which we can infer from Sections 2 and 3 have a larger signal over the Pacific Ocean, the northeast, and the northern Atlantic. Bins that peak in August are more evenly dispersed across the study domain, exhibiting no apparent relationship with surface type or latitude.

While most bins peak during the growing season, some spatially coherent bins peak in the winter (December and January). Though weaker than the summertime gradient, advection across the reverse wintertime gradient could be responsible for high synoptic XCO_2 variability in these bins. We observe cold season bins primarily over the northern Midwest, the northeast, and California. Peak cold season variability could reflect a relatively stronger wintertime gradient, more weather mixing, or higher variability in winter emissions, either local or transported, for these bins. For California and adjacent ocean bins (Figure 4b), which peaks primarily in Nov-Dec-Jan, high wintertime anthropogenic emissions from densely populated regions of California are mixing more with mean low latitude, CO_2-depleted winds flowing east. This contrasts with high wintertime emissions sources in the northeast, where mean winds flowing east from high

latitudes are already CO_2-enriched so there is only a weak concentration gradient. This is likely why areas like New York City and the DC area do not reach peak synoptic variability in the wintertime.

Synoptic XCO2 variance is greatest during winter months for ocean bins along the California coast (Figure 4b), which could be due to wintertime gradient mixing described above or to regional variability in air-sea CO2 fluxes. From December to February, strong and variable winds act on the central and northern California coast, causing intense mixing, sporadic upwelling events and variable sea surface temperatures (Garcia-Reyes and Largier, 2012). These are stormy months for the adjacent continent as well; Washington to California experiences the most intense synoptic weather from November to February. We see in Figure 4b coastal bins above California that reach peak variance in the wintertime. Inland areas experience the most intense synoptic weather in the early Spring, though no inland bins reach peak synoptic XCO2 variance then.

For the lower latitude Atlantic Ocean, in bins below 40 N, there are a few bins that reach peak variance in November. XCO_2 over this region of the Atlantic is impacted relatively more by the trade winds, which bring easterly, CO_2-depleted, low latitude air during the winter months. The amount of mixing across this early winter gradient, therefore, is on par with the amount of mixing across the summertime gradient for the lower-latitude Atlantic. For the lower latitude Pacific Ocean below 40 N, relative to the Atlantic, there are fewer bins that peak in November and more bins that peak in October. The wintertime gradient is likely less strong in the Pacific because wintertime emissions from Mexico and North America can get entrained in the trade winds and increase Pacific

Ocean wintertime XCO_2. This is reflected in Figure 1, where the lower latitude Pacific Ocean has a more positive spatial mean than the lower latitude Atlantic Ocean.

Bins that peak in May are less common, but occur over the Pacific Ocean, lower Atlantic Ocean, and one bin over Pennsylvania. Freshwater discharge into the Atlantic is greatest in May (Dai and Trenberth, 2002), which could induce variability in air-sea fluxes and therefore variability in XCO2. There are also some bins that peak in April over the Pacific Ocean. Perhaps the mean decreasing north-south gradient is stronger during the spring in those areas, or perhaps there is more April weather and therefore more mixing. This explanation is also possible for bins that peak in March, which mostly occur over the continental north and northern Atlantic.

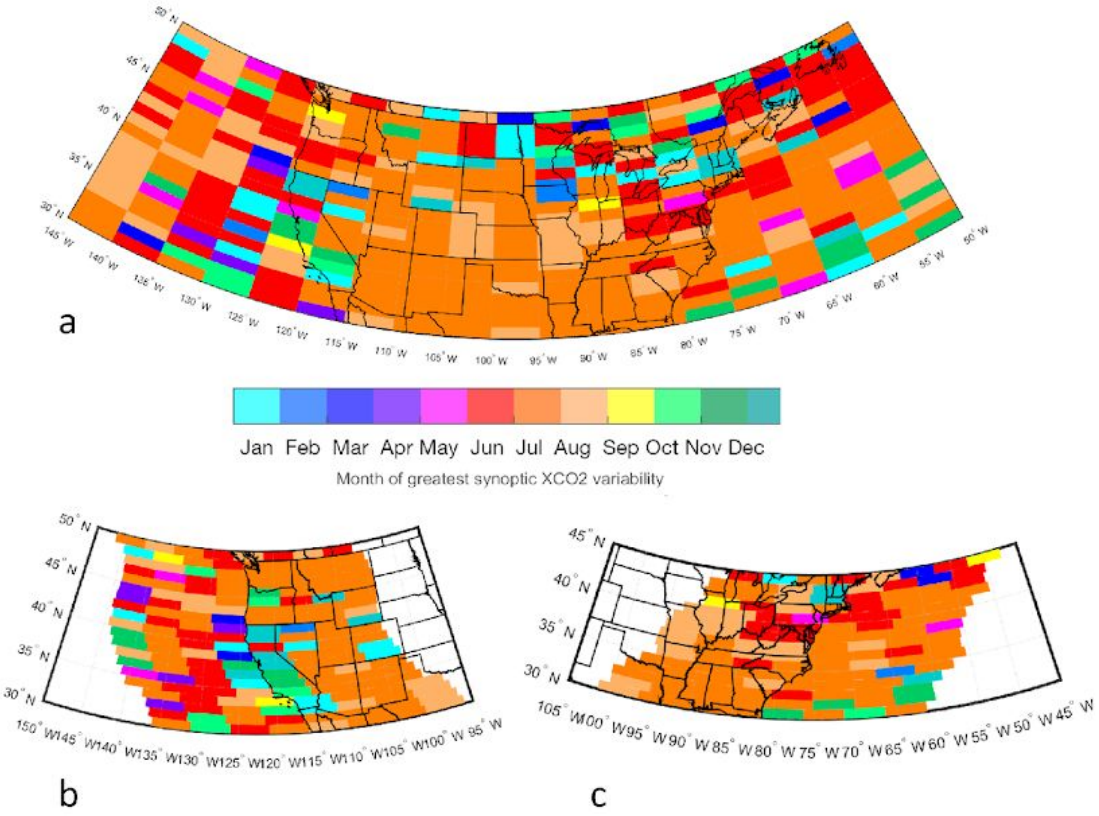

Figure 4. Figure 4a is a spatial map showing the months of peak synoptic XCO_2 variability for grid cells that are divided across the western United States coastline into 4 ocean bins and 4 land bins for each latitudinal band. Figure 4b is a spatial map showing the months of peak synoptic XCO_2 variability for grid cells that are divided across the eastern United States coastline into 4 ocean bins and 4 land bins for each latitudinal band.

5.5 Synoptic XCO_2 Anomaly Skewness

Overall, synoptic XCO_2 anomalies are distributed normally around their mean, with a full domain average skewness of -0.1 ppm, which is small in magnitude relative to

the full domain average synoptic XCO_2 variance of 1.5 ppm^2. The average skewness of land bins is 0.0 ppm for the east coast and 0.1 ppm for the west coast. Ocean bins are slightly negatively skewed, with an average skewness of -0.4 ppm for the west coast and -0.3 ppm for the east coast. The most positive skewness of any bin is 1.9 ppm and the most negative skewness is -1.2 ppm. Both bins are over the northern Atlantic Ocean, indicating that region may be more heavily influenced by outliers.

5.6 Summary of XCO_2 Statistical Parameters

The following tables summarize land-ocean, east-west, and north-south features of different XCO_2 parameters. There are separate tables for the full study domain, east coast, and west coast analyses.

Table 1. Statistical parameters for bins across the full study domain, averaged spatially into groups and across 1-degree latitude bands. The general Pacific Ocean region is represented by averaging XCO_2 from 145 – 125 W, the western half of the U.S. is represented by averaging from 125 – 100 W, and the combined eastern half of the U.S. and Atlantic Ocean are represented by averaging from 100-50 W. Northern bins are represented by averaging 40 – 50 N and southern bins by averaging 30 – 40 N.

Bin Group Averages	Detrended XCO_2 Spatial Mean (ppm)	XCO_2 Seasonal Amplitude (ppm)	XCO_2 Synoptic Anomaly Variance (ppm^2)	XCO_2 Synoptic Anomaly Skewness (ppm)	Month of Greatest Synoptic Variability
All bins	-0.3	7.8	1.5	-0.1	7
145 - 125 W	-0.1	8.1	1.1	-0.4	6
125 - 100 W	-0.3	6.3	1.8	0.1	7
100 - 50 W	-0.4	8.4	1.6	-0.2	7
30 - 40 N	-0.2	7.9	1.2	-0.3	7
40 - 50 N	-0.8	8.6	1.8	-0.1	7
49 – 50 N	-1.0	8.5	2.0	-0.2	6
48 – 49 N	-1.0	10.9	1.9	-0.2	6
47 – 48 N	-0.9	9.2	2.0	-0.1	6
46 – 47 N	-0.9	8.7	2.1	-0.2	6
45 – 46 N	-0.7	8.5	2.1	-0.2	7
44 – 45 N	-0.7	8.1	2.0	-0.1	7
43 – 44 N	-0.8	8.1	1.7	0.0	7
42 – 43 N	-0.7	8.0	1.6	-0.1	7
41 – 42 N	-0.7	7.9	1.5	0.0	7
40 – 41 N	-0.5	7.8	1.6	-0.1	7
39 – 40 N	-0.3	7.7	1.5	-0.2	7
38 – 39 N	0.0	7.5	1.5	-0.1	7
37 – 38 N	0.0	7.2	1.3	-0.2	7
36 – 37 N	0.2	7.2	1.3	-0.2	7
35 – 36 N	0.2	7.1	1.2	-0.2	7
34 – 35 N	0.3	6.8	1.2	-0.1	7
33 – 34 N	0.4	6.7	1.1	-0.2	7
32 – 33 N	0.3	6.7	1.0	-0.2	7
31 – 32 N	0.4	6.6	1.0	-0.2	7
30 – 31 N	0.4	6.6	1.0	-0.2	7

Table 2. Statistical parameters for *land* bins aligned with the west coast of the United States, averaged across 1-degree latitude bands.

Latitude Band (bottom bound)	Detrended XCO_2 Spatial Mean (ppm)	XCO_2 Seasonal Amplitude (ppm)	XCO_2 Synoptic Anomaly Variance (ppm^2)	XCO_2 Synoptic Anomaly Skewness (ppm)	Month of Greatest Synoptic Variability
49 – 50 N	-0.9	6.9	2.7	-0.1	6
48 – 49 N	-1.1	7.4	2.6	-0.1	7
47 – 48 N	-1.1	7.3	2.4	0.1	7
46 – 47 N	-0.9	7.2	2.5	0.1	7
45 – 46 N	-1.0	6.7	2.7	0.0	7
44 – 45 N	-1.0	6.5	2.7	-0.1	6
43 – 44 N	-1.1	6.5	2.4	0.0	7
42 – 43 N	-0.9	6.1	2.2	0.0	7
41 – 42 N	-0.7	6.1	2.0	0.1	12
40 – 41 N	-0.4	5.9	2.2	0.0	7
39 – 40 N	-0.3	5.8	2.1	0.0	7
38 – 39 N	-0.1	6.0	1.9	-0.1	7
37 – 38 N	0.0	6.0	1.6	0.1	7
36 – 37 N	0.2	6.0	1.5	0.1	7
35 – 36 N	0.1	5.8	1.3	0.2	7
34 – 35 N	0.4	5.7	1.6	0.3	7
33 – 34 N	0.4	5.9	1.2	0.2	7
32 – 33 N	0.3	5.9	1.1	0.3	8
31 – 32 N	0.3	5.9	1.1	0.1	7
30 – 31 N	0.3	6.0	1.2	0.1	7
Average Land	-0.4	6.3	1.9	0.1	7

Table 3. Statistical parameters for *ocean* bins aligned with the west coast of the United States, averaged across 1-degree latitude bands.

Latitude Band (bottom bound)	Detrended XCO_2 Spatial Mean (ppm)	XCO_2 Seasonal Amplitude (ppm)	XCO_2 Synoptic Anomaly Variance (ppm^2)	XCO_2 Synoptic Anomaly Skewness (ppm)	Month of Greatest Synoptic Variability
49 – 50 N	-0.3	8.9	1.1	-0.3	7
48 – 49 N	-0.2	9.2	1.0	-0.4	1
47 – 48 N	-0.5	8.9	1.3	-0.5	8
46 – 47 N	-0.3	9.0	1.1	-0.3	6
45 – 46 N	-0.3	8.9	1.4	-0.5	7
44 – 45 N	-0.4	8.4	1.5	-0.4	8
43 – 44 N	-0.4	8.4	1.2	-0.4	8
42 – 43 N	-0.2	8.1	1.1	-0.3	7
41 – 42 N	-0.4	8.0	1.0	-0.3	1
40 – 41 N	-0.4	8.5	1.0	-0.6	6
39 – 40 N	-0.2	8.3	0.9	-0.6	1
38 – 39 N	-0.1	7.8	1.0	-0.4	3
37 – 38 N	-0.1	7.5	0.9	-0.4	6
36 – 37 N	0.3	7.6	0.9	-0.4	6
35 – 36 N	0.2	7.5	0.9	-0.2	1
34 – 35 N	0.4	7.3	0.9	-0.2	6
33 – 34 N	0.5	7.2	1.0	-0.3	6
32 – 33 N	0.4	7.4	0.8	-0.3	4
31 – 32 N	0.6	7.3	0.8	-0.2	6
30 – 31 N	0.6	7.2	0.7	-0.4	7
Average Ocean	-0.1	8.1	1.0	-0.4	5

Table 4. Statistical parameters for bins aligned with the east coast of the United States, averaged across 1-degree latitude bands. Land bins are shaded in gray.

Latitude Band (bottom bound)	Detrended XCO_2 Spatial Mean (ppm)	XCO_2 Seasonal Amplitude (ppm)	XCO_2 Synoptic Anomaly Variance (ppm^2)	XCO_2 Synoptic Anomaly Skewness (ppm)	Month of Greatest Synoptic Variability
44 – 45 N	-0.7	9.1	2.3	0.1	6
43 – 44 N	-0.8	9.0	2.1	0.0	7
42 – 43 N	-0.7	8.8	1.9	0.0	7
41 – 42 N	-0.6	9.2	1.8	0.2	6
40 – 41 N	-0.2	8.9	1.8	-0.1	8
39 – 40 N	0.0	9.1	1.7	0.1	6
38 – 39 N	0.2	8.6	1.9	0.1	6
37 – 38 N	0.3	7.8	1.6	0.1	8
36 – 37 N	0.6	7.7	1.8	-0.1	8
35 – 36 N	0.7	8.0	1.7	-0.1	7
34 – 35 N	0.7	7.2	1.7	-0.1	7
33 – 34 N	0.8	6.5	1.5	-0.1	7
32 – 33 N	0.7	6.6	1.4	-0.2	7
31 – 32 N	0.7	6.1	1.5	-0.2	7
30 – 31 N	0.8	6.0	1.6	0.1	7
Average Land	0.2	7.9	1.7	0.0	7
44 – 45 N	-0.6	9.1	1.4	0.0	3
43 – 44 N	-1.1	9.0	1.1	0.2	6
42 – 43 N	-1.1	9.2	1.1	0.0	6
41 – 42 N	-1.2	8.4	1.1	-0.1	7
40 – 41 N	-1.0	8.6	1.5	0.2	6
39 – 40 N	-0.6	8.1	1.3	-0.7	7
38 – 39 N	0.0	7.9	1.1	-0.4	7
37 – 38 N	-0.1	8.0	1.1	-0.4	7
36 – 37 N	-0.3	7.7	1.1	-0.7	7
35 – 36 N	-0.1	7.5	1.0	-0.7	7
34 – 35 N	0.1	7.2	0.9	-0.5	7
33 – 34 N	0.1	6.8	0.9	-0.3	7
32 – 33 N	0.2	6.5	0.9	-0.5	7
31 – 32 N	0.2	6.7	0.9	-0.4	7
30 – 31 N	0.2	6.8	0.8	-0.4	7
Average Ocean	-0.4	7.8	1.1	-0.3	7

5.7 Glint Mode Only Analysis

We compared the analysis using combined glint and nadir pointing mode observations to an analysis only using glint mode observations to examine how pointing mode impacted our results. We found differences between the analyses to be mostly insignificant, with the exception of a 0.9 ppm difference in seasonal amplitudes for the 45-46 N latitude band. Additionally, above 48 N, synoptic anomaly variances tended to be ~20% lower when only using glint mode observations. Glint mode observations are more susceptible to cloud encounters due to their longer paths through the atmosphere, which are generally more prevalent the higher latitudes of our study domain.

Table 5. Differences in statistical parameters following the west coast of the United States (glint parameter - glint+nadir parameter). Positive values indicate using glint mode observations only increases the parameter relative to using both glint and nadir mode observations.

Latitude Band (bottom bound)	Detrended XCO_2 Spatial Mean (ppm)	XCO_2 Seasonal Amplitude (ppm)	XCO_2 Synoptic Anomaly Variance (ppm^2)	XCO_2 Synoptic Anomaly Skewness (ppm)
49 – 50 N	0.1	0.1	-0.4	0.2
48 – 49 N	0.2	-0.2	-0.3	0.1
47 – 48 N	0.3	0.1	-0.4	0.0
46 – 47 N	0.0	0.0	-0.2	-0.2
45 – 46 N	0.1	0.9	-0.1	0.0
44 – 45 N	0.2	0.1	-0.2	0.0
43 – 44 N	0.0	0.2	-0.1	-0.1
42 – 43 N	0.0	-0.1	-0.1	-0.1
41 – 42 N	0.0	0.1	0.1	0.0
40 – 41 N	0.1	-0.1	-0.2	-0.1
39 – 40 N	0.2	-0.1	0.0	0.2
38 – 39 N	0.0	0.0	-0.1	0.2
37 – 38 N	0.1	0.1	0.0	0.1
36 – 37 N	0.2	0.0	0.0	0.0
35 – 36 N	0.2	0.0	0.0	-0.1
34 – 35 N	0.0	0.0	-0.3	-0.1
33 – 34 N	0.2	0.0	0.0	-0.1
32 – 33 N	0.2	-0.1	0.0	-0.2
31 – 32 N	0.1	-0.2	0.0	-0.1
30 – 31 N	0.1	0.1	0.0	-0.1
Average West	0.1	0.0	-0.1	0.0

Table 6. Differences in statistical parameters following the east coast of the United States (glint parameter - glint+nadir parameter). Positive values indicate using glint mode observations only increases the parameter relative to using both glint and nadir mode observations.

Latitude Band (bottom bound)	Detrended XCO_2 Spatial Mean (ppm)	XCO_2 Seasonal Amplitude (ppm)	XCO_2 Synoptic Anomaly Variance (ppm^2)	XCO_2 Synoptic Anomaly Skewness (ppm)
44 – 45 N	0.1	-0.1	-0.2	-0.1
43 – 44 N	0.0	0.3	-0.2	-0.2
42 – 43 N	-0.1	0.0	-0.1	0.0
41 – 42 N	0.1	0.0	-0.1	0.0
40 – 41 N	0.1	0.0	-0.1	0.1
39 – 40 N	0.0	0.0	0.0	0.0
38 – 39 N	0.1	0.0	0.0	0.0
37 – 38 N	0.0	0.2	0.0	-0.1
36 – 37 N	0.0	0.0	-0.1	-0.1
35 – 36 N	0.1	0.0	0.0	-0.1
34 – 35 N	0.0	0.1	0.0	0.0
33 – 34 N	0.0	0.1	0.0	0.0
32 – 33 N	0.0	0.0	0.0	-0.1
31 – 32 N	0.0	0.1	0.0	-0.1
30 – 31 N	0.0	0.0	0.0	-0.1
Average East	0.0	0.0	-0.1	-0.1

5.8 Impact of Small-Scale Spatial Correlation

By averaging along the orbit track and repeating the analysis, we estimate the amount of variance imparted by instrument/algorithm noise or small-scale spatial geophysical signals to contribute about a quarter of overall synoptic XCO_2 variance. The orbit averaging technique increases the fraction of independent XCO_2 observations and thus reflects actual variance more robustly. Spatially correlated variance contributes more to the overall variance budget over land than ocean by about 1%. The spatially correlated

component of variance does not affect the large-scale trends observed in the analysis. As mentioned in Section 4.3, in further research we will use a band pass filtering technique to better constrain this component of variability within the synoptic XCO_2 anomalies.

6. Summary

Geographic patterns in the mean spatial distribution and temporal variations in atmospheric XCO_2 reflect a combination of surface carbon fluxes and large-scale atmospheric circulation. The relative influence of these mechanisms vary across the study domain and for the different features of XCO_2. The decreasing pattern in detrended OCO-2 XCO_2 means from 30 N to 50 N is consistent with findings from GOSAT, TCCON, and modeled XCO_2 (Liang et al., 2017; Jing et al., 2018). Therefore, the spatial distribution of XCO_2 when averaged over full seasonal cycles reflect mean east-west atmospheric transport of the growing seasonal meridional gradient more directly than local surface carbon fluxes. The horizontal atmospheric winds smoothing east-west variations is exemplified in the lack of a contrast between adjacent land and ocean bin means. Integration of the full North American terrestrial drawdown for air off the east coast could be the driver of more negative ocean XCO_2 means over the Atlantic than the Pacific.

Seasonal variability in XCO_2 reflects seasonality in local carbon fluxes as well as transported variability from regions atmospherically upstream. The dominant continental pattern in seasonal amplitudes is low over the western U.S. and greater over the eastern

U.S., consistent with seasonality in underlying surface CO_2 fluxes, which have a greater seasonality in the more vegetated eastern United States. However, other patterns observed in the seasonal amplitudes are not consistent with the seasonality expected from underlying biospheric surface fluxes, illustrating where XCO_2 seasonal variability is heavily influenced by transported variability as opposed to local fluxes. This feature emerges when we observe greater seasonal amplitudes over the northern Pacific Ocean compared to the adjacent forested Pacific northwest and greater amplitudes observed over less productive Canadian Shield compared to more productive southeastern states such as Mississippi. A continuous, mostly meridional band of highly seasonal variable air induced by aggregated boreal surface fluxes around the globe was found by Sweeney et al., (2015). This highly seasonal boreal air seems to be contributing to the greater seasonal XCO_2 amplitudes over the northern Pacific Ocean, the northeastern continent, and the northern Atlantic Ocean. Adjacent land and ocean similarities in seasonal amplitudes are observed over the east, signifying the Atlantic Ocean more closely reflects North American seasonal carbon cycling while the Pacific seasonal XCO_2 cycle is more influenced by transported variability from other continents.

For most bins, synoptic XCO_2 variance is greatest in the summer, reinforcing findings from Keppel-Aleks et al., (2011) that synoptic-scale XCO_2 variations are primarily driven by advection across the meridional growing season spatial gradient. Bins with the greatest synoptic XCO_2 variance are located above the continental northwest and northeast (2-3 ppm^2) and have peak variance in the summer. While most bins in the domain have greatest synoptic XCO_2 variance during July, most bins from 45-50 N peak

in June, potentially reflecting an earlier start of the boreal growing season, observed in Chen and Yang (2020).

Land bins have higher synoptic variances on average than ocean bins, possibly resulting from spatial variability in local fluxes as well as the stronger spatial gradient we observe over land in Figure 1. There could also be a land-ocean retrieval bias, which we plan to investigate in future work using retrieval covariates. For bins aligned along the western coastline, there is a clear contrast in synoptic XCO_2 anomaly variance for adjacent land and ocean bins, resembling the contrast we observe in seasonal amplitudes. Compared to the northwest coast, there seems to be more east-west smoothing of XCO_2 across the east coast, and the continental signal tracks out over the Atlantic Ocean as observed in the seasonal amplitudes.

There is a surprising amount of synoptic XCO_2 variance over the northwest, given the XCO_2 transport simulated by Jing et al., (2018) which shows less large scale eddies acting on the region. These high variance bins have a spatial correlation with topography, suggesting that retrieval bias, mountain meteorology, or biological flux variability owing to the treeline can drive significant variations in synoptic-scale XCO_2. The possible topography effect on synoptic XCO_2 variance is not observed over the lower elevation Applachian range.

Though weaker than the summertime gradient, advection across the reverse wintertime gradient can also induce synoptic XCO_2 variance. Peak cold season variability, primarily observed over the northern Midwest, the northeast, California and

its adjacent coastal ocean could reflect a relatively stronger wintertime gradient, storm-induced air-sea flux variability, more weather mixing, or higher variability in winter emissions, either local or transported, for these bins. For the lower latitude Atlantic Ocean (below 40 N), some bins have peak synoptic variance in November, suggesting a strong influence of the trade winds, which bring easterly, CO_2-depleted air frow lower latitudes during the winter. The high variance bin over Los Angeles peaks in October, and could be tied to the mixing of dense local wintertime anthropogenic fluxes with CO_2-depleted air flowing east from lower latitudes. This mixing could be exacerbated by the Sierra Nevada range trapping emissions in western California. There are dense wintertime emissions sources in the northeast, but mean winds flowing east from high latitudes are already CO_2-enriched, creating only a weak concentration gradient. This is likely why areas like New York City and the DC area do not reach peak synoptic variability in the wintertime.

7. Conclusions and Future Directions

Mean east-west transport of strong growing season CO_2 drawdown outweighs the strong wintertime emissions in northern latitudes, creating the net negative, increasing north-south mean detrended XCO_2 gradient over the study domain. We observe east-west smoothing of land and ocean XCO_2 distributions for both coasts in detrended XCO_2 means. For seasonal and synoptic scale variability, this smoothing is not present across the northwestern coast. The pattern of high XCO_2 seasonal amplitudes reflect the meridional transport path of northern latitude boreal fluxes, which seem to have a larger signal over the Pacific Ocean, get deflected off the northwestern coast, and dip back

down over the northeast and adjacent northern Atlantic. The continental signal for seasonal amplitudes and synoptic variance tracks out over the northern Atlantic Ocean. Seasonality in the northern Atlantic Ocean's air-sea fluxes could induce variability as well, but they are not large enough to entirely produce the amplitudes we observe. The dominant patterns in synoptic XCO_2 variance are driven by advection across the meridional growing season gradient, but advection across the weaker reverse wintertime gradient affects could be more important for some southern regions. Variability in air-sea flux for the California coastal ocean during the stormy winter season could also be a large contributor to the region's synoptic variance. Over the Pacific Northwest, topography may induce synoptic-scale XCO_2 variations. Patterns in variability for land and ocean XCO_2 are very uniform across the northeastern coast while heavily contrasted across the northwestern coast.

Our results show that there is a spatially and temporally variable influence of local fluxes (biosphere, air-sea, human-mediated), XCO_2 transported from boreal regions (either North American or from other continents), and advection across large-scale spatial gradients (growing season or wintertime) in XCO_2. In further work, we aim to diagnose and quantify the mechanisms of XCO_2 variability uncovered in this study. We can use HYSPLIT-2, an atmospheric back trajectory model to determine the origin of XCO_2 anomalies of interest. This can help explain the high synoptic XCO_2 variance we observe in different regions and help us identify any potential measurement biases (such as a topography or land-ocean related bias). It will also help us identify the relative contribution of North American seasonal variability versus variability transported from

another continent for different regions in the study domain. Our investigation into the different drivers of XCO_2 variability at seasonal and sub-seasonal scales provides new and relevant insight into the carbon cycle. These insights may be useful in efforts that leverage atmospheric CO_2 observations for flux inference.

8. References

Baker, D. F., et al. "Carbon source/sink information provided by column CO 2 measurements from the Orbiting Carbon Observatory." *Atmospheric Chemistry & Physics* 10.9 (2010).

Baker, David F., Scott C. Doney, and David S. Schimel. "Variational data assimilation for atmospheric CO_2." *Tellus B: Chemical and Physical Meteorology* 58.5 (2006): 359-365.

Chatterjee, A., et al. "Influence of El Niño on atmospheric CO_2 over the tropical Pacific Ocean: Findings from NASA's OCO-2 mission." *Science* 358.6360 (2017): eaam5776.

Chen, Xiaona, and Yaping Yang. "Observed earlier start of the growing season from middle to high latitudes across the Northern Hemisphere snow-covered landmass for the period 2001–2014." Environmental Research Letters 15.3 (2020): 034042.

Crisp, David, et al. "The ACOS CO_2 retrieval algorithm-Part II: Global XCO_2 data characterization." (2012): 687.

Crisp, David, et al. "The orbiting carbon observatory (OCO) mission." *Advances in Space Research* 34.4 (2004): 700-709.

Dai, Aiguo, and Kevin E. Trenberth. "Estimates of freshwater discharge from continents: Latitudinal and seasonal variations." Journal of hydrometeorology 3.6 (2002): 660-687.

Eldering, A., et al. "The Orbiting Carbon Observatory-2 early science investigations of regional carbon dioxide fluxes." *Science* 358.6360 (2017): eaam5745.

Fennel, K., et al. "Carbon cycling in the North American coastal ocean: a synthesis" *Biogeosciences* 16 (2019): 1281-1304.

García-Reyes, M., and J. L. Largier. "Seasonality of coastal upwelling off central and northern California: New insights, including temporal and spatial variability." Journal of Geophysical Research: Oceans 117.C3 (2012).

Geels, C., et al. "Investigating the sources of synoptic variability in atmospheric CO_2 measurements over the Northern Hemisphere continents: a regional model study." *Tellus B: Chemical and Physical Meteorology* 56.1 (2004): 35-50.

Hayes, D. J., et al. "Chapter 2: the North American carbon budget." *Second State of the Carbon Cycle Report (SOCCR2): A Sustained Assessment Report. US Global Change Research Program, Washington, DC, USA* (2018): 71-108.

Jing, Yingying, et al. "Global atmospheric CO_2 concentrations simulated by GEOS-Chem: Comparison with GOSAT, carbon tracker and ground-based measurements." Atmosphere 9.5 (2018): 175.

Keppel-Aleks, G., P. O. Wennberg, and T. Schneider. "Sources of variations in total column carbon dioxide." *Atmospheric Chemistry and Physics* 11.8 (2011): 3581-3593.

Kiel, Matthäus, et al. "How bias correction goes wrong: measurement of XCO_2 affected by erroneous surface pressure estimates." Atmospheric Measurement Techniques 12.4 (2019).

Lareau, Neil P., and John D. Horel. "The climatology of synoptic-scale ascent over western North America: A perspective on storm tracks." Monthly weather review 140.6 (2012): 1761-1778.

Liang, Ailin, et al., "Comparison of Satellite-Observed XCO_2 from GOSAT, OCO-2, and Ground-Based TCCON." Remote Sensing 9.10 (2017):1033

Marcotullio, P. J., et al., "Chapter 3: Energy systems" Second State of the Carbon Cycle Report (SOCCR2): A Sustained Assessment Report. US Global Change Research Program, Washington DC, USA (2018): 110-188

Massie, Steven T., et al. "Observational evidence of 3‐D cloud effects in OCO‐2 CO_2 retrievals." Journal of Geophysical Research: Atmospheres 122.13 (2017): 7064-7085.

Northcott, Devon, et al. "Impacts of urban carbon dioxide emissions on sea-air flux and ocean acidification in nearshore waters." *PloS one* 14.3 (2019).

O'Dell, Christopher, et al. "Improved retrievals of carbon dioxide from Orbiting Carbon Observatory-2 with the version 8 ACOS algorithm." (2018): 6539.

Olsen, Seth C., and James T. Randerson. "Differences between surface and column atmospheric CO_2 and implications for carbon cycle research." Journal of Geophysical Research: Atmospheres 109.D2 (2004).

Parazoo, N. C., et al. "Moist synoptic transport of CO_2 along the mid‐latitude storm track." *Geophysical Research Letters* 38.9 (2011).

Sitch, Stephen, et al. "Recent trends and drivers of regional sources and sinks of carbon dioxide." *Biogeosciences* 12.3 (2015): 653-679.

Stubenrauch, C. J., et al. "A 6-year global cloud climatology from the Atmospheric InfraRed Sounder AIRS and a statistical analysis in synergy with CALIPSO and CloudSat." (2010).

Sweeney, Colm, et al. "Seasonal climatology of CO_2 across North America from aircraft measurements in the NOAA/ESRL Global Greenhouse Gas Reference Network." Journal of Geophysical Research: Atmospheres 120.10 (2015): 5155-5190.

Torres, Anthony D., et al. "A geostatistical framework for quantifying the imprint of mesoscale atmospheric transport on satellite trace gas retrievals." *Journal of Geophysical Research: Atmospheres* 124.17-18 (2019): 9773-9795.

Zhang, Yao, et al. "A global moderate resolution dataset of gross primary production of vegetation for 2000–2016." Scientific data 4 (2017): 170165.